Article:
Pal, A, Potjer, TP, Thomsen, SK et al. (12 more authors) (2016) Loss-of-Function Mutations in the Cell-Cycle Control Gene CDKN2A Impact on Glucose Homeostasis in Humans. Diabetes, 65 (2). pp. 527-533. ISSN 0012-1797

https://doi.org/10.2337/db15-0602

Loss-of-Function Mutations in the Cell-Cycle Control Gene *CDKN2A* Impact on Glucose Homeostasis in Humans

Short running title: The role of *CDKN2A* in glucose homeostasis

Aparna Pal[1]*, Thomas P. Potjer[2]*, Soren K. Thomsen[1]*, Hui Jin Ng[1], Amy Barrett[1], Raphael Scharfmann[3], Tim J. James[4], D. T. Bishop[5], Fredrik Karpe[1,6], Ian F. Godsland[7], Hans F.A. Vasen[8], Julia Newton-Bishop[5], Hanno Pijl[9], Mark I. McCarthy[1,6,10], Anna L. Gloyn[1,6]

*A.P, T.P.P and S.K.T. are joint first authors.

1) Oxford Centre for Diabetes Endocrinology & Metabolism, University of Oxford, UK

2) Department of Clinical Genetics, Leiden University Medical Center, Leiden, Netherlands

3) INSERM U1016, Institut Cochin, Université Paris Descartes, Paris, France

4) Department of Clinical Biochemistry, John Radcliffe Hospital, Oxford, UK

5) Leeds Institute of Cancer & Pathology, University of Leeds, Leeds, UK

6 Oxford NIHR Biomedical Research Centre, Churchill Hospital, Oxford, UK

7) Diabetes, Endocrinology and Metabolism, Department of Medicine, Imperial College London, London, UK

8) Department of Gastroenterology & Hepatology, Leiden University Medical Center, Leiden, Netherlands

9) Leiden University Medical Centre, Department of Internal Medicine, Leiden, Netherlands

10) Wellcome Trust Centre for Human Genetics, University of Oxford, UK

Address for Correspondence

Professor Anna L Gloyn
Oxford Centre for Diabetes Endocrinology & Metabolism
Churchill Hospital, Oxford, OX3 7LE, UK
Tel:- +44 1865 857298
Fax:- +44 1865 857299
Email:- Anna.Gloyn@drl.ox.ac.uk

Number of Tables: 2

Number of Figures: 2

Diabetes Publish Ahead of Print, published online November 5, 2015

Abstract

At the *CDKN2A/B* locus, three independent signals for type 2 diabetes risk are located in a non-coding region near *CDKN2A*. The disease-associated alleles have been implicated in reduced β-cell function, but the underlying mechanism remains elusive. In mice, β-cell specific loss of *Cdkn2a* causes hyperplasia whilst overexpression leads to diabetes, highlighting *CDKN2A* as a candidate effector transcript. Rare *CDKN2A* loss-of-function mutations are a cause of familial melanoma and offer the opportunity to determine the impact of *CDKN2A* haploinsufficiency on glucose homeostasis in humans. To test the hypothesis that such individuals have improved β-cell function, we performed oral and intravenous glucose tolerance tests on mutation carriers and matched controls. Compared with controls, carriers displayed increased insulin secretion, impaired insulin sensitivity and reduced hepatic insulin clearance. These results are consistent with a model whereby *CDKN2A*-loss affects a range of different tissues, including pancreatic β-cells and liver. To test for direct effects of *CDKN2A*-loss on β-cell function, we performed knockdown in a human β-cell line, EndoC-bH1. This revealed increased insulin secretion independent of proliferation. Overall, we demonstrate that *CDKN2A* is an important regulator of glucose homeostasis in humans, thus supporting its candidacy as an effector transcript for type 2 diabetes-associated alleles in the region.

Introduction

Non-coding genetic signals at the CDKN2A/B locus have been associated with increased risk of developing type 2 diabetes (1, 2). One signal is contained within a long non-coding RNA (*ANRIL*), while two distinct signals map to a region located further upstream of *CDKN2A* and *CDKN2B*. Physiological characterisations of normoglycemic carriers have demonstrated that the risk alleles are associated with reduced β-cell function, yet the underlying 'effector' transcript driving these effects has not been established (3, 4).

CDKN2A encodes the alternatively spliced proteins $p16^{INK4a}$ and $p14^{ARF}$, which are known tumour suppressors acting via distinct signalling pathways (5, 6). $p16^{INK4a}$ is a cyclin-dependent kinase inhibitor (CDKI) involved in the regulation of cell cycle progression through inhibition of CDK4 and CDK6 (7). $p14^{ARF}$, in contrast, prevents the degradation of the cell-cycle regulator p53 by forming a stable complex with Mdm2 in the nucleus (8).

Rodent studies have linked *Cdkn2a* to glucose homeostasis, pointing to the gene as a plausible candidate effector transcript at the *CDKN2A/B* locus. In a β-cell specific knockout mouse, *Cdkn2a* deficiency was found to increase β-cell proliferation and conferred resistance to chemically-induced diabetes (9). Overexpression, in contrast, reduced β-cell proliferation in both young and old mice. This is consistent with the effect of *Cdk4*-loss, which has been shown to result in a reduced number of pancreatic β-cells and insulin-deficient diabetes (10). More recent mouse studies have also established a role for *Cdkn2a* and *Cdk4* in hepatic glucose production (HGP), demonstrating cell-cycle independent effects on gluconeogenesis under fasted and fed conditions (11, 12).

While rodent studies have provided critical clues into the contribution of *Cdkn2a* to diabetes pathogenesis, less is known about the role of *CDKN2A* in glucose homeostasis in humans. The machinery regulating the G1/S transition in adult human β cells differs from

that of mouse β cells, which do not express CDK6 (13-15). Individuals heterozygous for germline loss-of-function mutations in the *CDKN2A* gene have a high risk of developing (multiple) cutaneous melanoma, a condition known as familial atypical multiple mole melanoma syndrome (FAMMM) (16, 17). These subjects provide a unique opportunity to study the effect of *CDKN2A* haploinsufficiency on glucose homeostasis in humans. The present study tested the hypothesis that mutation carriers show improved β-cell function compared with non-carriers.

Research design and methods

Study participants

Thirty-one cases diagnosed with FAMMM due to *CDKN2A* mutations were recruited from centres in the UK and the Netherlands. Twenty-eight had been cancer free for at least two years, and the remaining three cases had presented with melanoma between four to twelve months prior to inclusion in the study (**supplementary table 1**). For a control group of thirty-one participants, unaffected first-degree relatives or spouses of carriers were chosen when available and additional controls were recruited from the Oxford Biobank (www.oxfordbiobank.org.uk). Two controls were subsequently excluded based on 2-h OGTT glucose levels diagnosing diabetes (serum glucose >11 mmol/L). All remaining participants were aged 18-80 years, not suffering from diabetes, and not taking any medication that could interfere with glucose tolerance.

Baseline clinical characteristics and oral glucose tolerance test (OGTT)

All participants underwent a 75 g OGTT following a 12 hour fast. Blood samples were collected at 0, 15, 30, 60, 90 and 120 min after the oral glucose load to assay plasma glucose, serum insulin and (for a subset of twelve mutation carriers and twelve controls) also C-peptide. Insulin and C-peptide were measured using chemiluminescence immunoassays. Measures of insulin sensitivity, β-cell function and hepatic clearance derived from the OGTT were calculated according to the formulae in **supplementary table 2**.

Intravenous glucose tolerance test (IVGTT)

IVGTTs were performed on a subset of the UK subjects (eight) who had attended for OGTT and consented to undergo an IVGTT. Control subjects, matched for age, gender, BMI and activity were recruited from the Oxford Biobank. Following a 12 hour fast, a dose of 50

% dextrose (calculated based on weight 0.5mg/kg) was given over 3 minutes. Blood samples were then taken at 0, 2, 4, 6, 8, 10, 15, 20, 30, 45, 60, 75, 90, 120, 150 and 180 minutes. These samples were batch-analysed for insulin, glucose and C-peptide. Data were then analysed using a minimal model approach, according to an algorithm designed to maximise precision and identification success rate (18).

Cellular assays using the EndoC-bH1cell line

The EndoC-bH1 cell line was cultured and passaged as previously described (19). Reverse transfections were performed by adding pre-formed siRNA complexes prepared from ON-TARGETplus siRNA SMARTpools (Dharmacon) at a final concentration of 10 nM siRNA. For gene expression analysis, RNA was extracted and quantitative PCR (qPCR) performed using the TaqMan gene expression kit and assays (Applied Biosystems) on oligo-dT primed cDNA. 72 h after transfection, cells were starved overnight in 2.8 mM glucose followed by 1 h in 0 mM glucose medium. Static insulin secretion assays were then initiated by adding glucose-free growth medium supplemented with the indicated amounts of glucose and IBMX. After 1 h, aliquots of supernatants were removed for later analysis, and ice-cold acid ethanol added to extract insulin content from cells. Sample analysis was performed using the AlphaLISA Human Insulin Immunoassay (Perkin Elmer).

For protein kinase A (PKA) activity assays, cells were harvested following knockdown, as described above, and washed in phosphate-buffered saline. Matching input for number of cells, the samples were then processed according to manufacturer's instructions for the PepTag non-radioactive PKA assay (Promega), and visualized using the ChemiDoc MP system.

Statistical analysis

Statistical analysis was performed using R 3.0.2. P-values were determined by Welch's t-test, except for gender differences where the Chi-squared test was used and for analysis of the IVGTT data where the Mann-Whitney U test was used.

Results

We recruited thirty-one participants carrying inherited *CDKN2A* loss-of-function mutations (**supplementary table 1**) and thirty-one controls, matched as a group for age (p = 0.99), gender (p = 0.43) and BMI (p = 0.97) (**table 1**). To test our hypothesis that *CDKN2A*-loss leads to improved β-cell function, we first performed a 120-min oral glucose tolerance test (OGTT) in all subjects (**figure 1a-b**). While no difference in glucose levels was detected, insulin levels were significantly increased in carriers throughout the test (p = 0.01 for insulin area under curve [AUC]; **table 2**).

Using these data, we derived standard indices of β-cell function and insulin sensitivity (**table 2**). This revealed increased β-cell function in carriers compared with non-carriers, both using a dynamic measure of acute insulin response (p = 0.03 for BIGTT-AIR), and in the fasted state (p = 0.05 for HOMA-B, homeostatic model assessment of β-cell function). Corresponding measures of insulin sensitivity, BIGTT-S and HOMA-S (homeostatic model assessment of insulin sensitivity), were also both found to be lower in carriers (p = 0.04 and p = 0.05, respectively). Other standard measures, the Belfiore and Matsuda ISIs, confirmed the observed reduction in insulin sensitivity of carriers (p = 0.02 and p = 0.02, respectively). As a result, the disposition index, which is an aggregate measure of β-cell function relative to glucose sensitivity, remained unaffected compared with controls (p = 0.98). These results were not significantly altered by exclusion of three carriers that had presented with melanoma within two years prior to inclusion in the study (**supplementary table 3**).

To explore whether the observed phenotype was driven by underlying effects on $p16^{INK4a}$, $p14^{ARF}$ or both, we re-analysed the data grouping carriers by mutation status (**supplementary figure 1**). Of the mutations identified, 26 affected both $p16^{INK4a}$ and $p14^{ARF}$, while five were located in regions affecting $p16^{INK4a}$ exclusively. No differences were observed between these two groups in insulin or glucose levels (p = 1.00 for AUC_{ins} and p =

0.49 for $AUC_{glucose}$, respectively), suggesting that the observed metabolic phenotype of mutation carriers may be driven either solely by effects on $p16^{INK4a}$, or by effects of similar magnitude on both proteins.

For a subset of participants (twelve carriers and twelve controls) C-peptide measurements were obtained during the OGTT. Despite a tendency towards increased C-peptide levels in the fasted state (p = 0.48), the total response was not different for this subset of individuals (p = 1.00 for AUC). Indices of hepatic insulin clearance, derived from the ratio between C-peptide and insulin levels, however, showed significantly decreased hepatic clearance in mutation carriers (p = 0.03; **table 2**) (20).

To confirm these findings, we performed IVGTTs on eight cases and eight controls available for follow-up studies (**supplementary figure 2**). None of the measures derived from this test reached statistical significance, but directions of effect were confirmed for both insulin secretion (p = 0.14 for $AUC_{insulin}$ 10-180 min) and hepatic insulin clearance (p = 0.21) (**supplementary table 4**). The insulin response was found to be 66 % and 110 % higher for carriers during the first and second phase of secretion, respectively. In contrast, the C-peptide response (which is unaffected by hepatic clearance) was around 30 % higher during both phases of secretion, indicating a direct contribution of improved β-cell function to the elevated circulating insulin levels of carriers.

Finally, we sought to establish the extent to which cell-cycle independent effects of *CDKN2A* on the regulation of insulin secretion could contribute to the phenotype of mutation carriers. Recent work in rodent hepatocyte models has suggested a role of *CDKN2A* in the regulation of protein kinase A (PKA) signalling (12). Given the well-characterised effects of PKA on potentiation of insulin secretion, we speculated that such signalling events could have a direct effect on β-cell function. To test this hypothesis, we performed knockdown and

secretion studies in the human pancreatic β-cell line, EndoC-bH1. This cell line was transformed by Ravassard et al using the proto-oncogene SV40LT, which acts on the Retinoblastoma protein (Rb), thereby masking effects of $p16^{INK4a}$ on cell-cycle control (19).

We first confirmed expression of $p16^{INK4a}$ by immunofluorescence and found that, consistent with previous reports, the protein localized to both the nucleus and cytoplasm (**supplementary figure 3**) (21, 22). siRNA-mediated silencing of *CDKN2A* was then performed and efficient knockdown observed both at the mRNA and protein level (**figure 2a-b; supplementary figure 4**). 96 hours after gene silencing, cells treated with *CDKN2A* or non-targeting siRNAs were incubated under different conditions to assess the glucose-responsiveness of the cells. In addition to basal and high-glucose conditions, the effect of the phosphodiesterase inhibitor (IBMX) on insulin secretion was tested. For all three conditions, *CDKN2A* knockdown was found to increase insulin secretion as a fraction of total content (basal, $p = 0.02$; high, $p = 0.01$; high glucose with IBMX, $p = 0.04$; **figure 2c-d**) and, as expected, no effect on proliferation was detected. We also observed a small, but significant reduction in the total insulin content per cell ($p < 0.01$; **supplementary figure 5**). Finally, we performed PKA activity assays to directly assess the effect of *CDKN2A* silencing on the potentiating pathway of insulin secretion. Consistent with an increase in insulin secretion, this revealed a corresponding 23 % increase in the activity of PKA following *CDKN2A* knockdown ($p = 0.02$; **supplementary figure 6**).

Discussion

Individuals carrying heterozygous loss-of-function mutations in the *CDKN2A* gene provide a unique opportunity to study the role of $p16^{INK4a}$ and $p14^{ARF}$ in glucose homeostasis in humans. Through oral and intravenous glucose tolerance tests, we found that carriers displayed significantly increased insulin levels compared with matched controls. In a subset

of individuals, measurements of C-peptide levels established a contribution of both decreased hepatic insulin clearance and increased β-cell function to the elevated circulating insulin. Further, grouping carriers by mutation status showed the effects to be driven either by $p16^{INK4a}$ exclusively or through similar effects on both $p16^{INK4a}$ and $p14^{ARF}$.

Overall, these results are consistent with a combination of two, non-mutually exclusive mechanisms underlying the phenotype of carriers: *(a)* primary β-cell hyperfunction driving progressive insulin resistance; and/or *(b)* primary insulin resistance triggering a compensatory increase in insulin levels (**supplementary figure 7**). While both explanations are consistent with our data, existing evidence strongly support a role for *CDKN2A* in β-cell function (9). Chronic hyperinsulinemia is known to result in a gradual down-regulation of both insulin receptors and post-receptor signalling efficiency, thereby causing general insulin resistance and reduced insulin clearance (23). Our data are therefore in agreement with the expected physiological adaption to chronic hyperinsulinemia. However, due to limitations on the design of our clinical study, we cannot conclusively address the cause and effect between hyperinsulinemia and insulin resistance in mutation carriers. The IVGTT is well validated against clamp-based techniques, but power calculations based on our results suggest that an impractically high number of 50-60 individuals would be required to establish significant differences. Given the rarity of the disease, this exceeds the number of carriers available in the UK and Dutch cohorts recruited for our study.

To test for a cell-cycle independent role of *CDKN2A* in the regulation of insulin secretion, we performed knockdown studies in the human β-cell line, EndoC-bH1. This identified cell-cycle independent increases in insulin secretion under three conditions. These changes were found to be accompanied by increased PKA activity, in agreement with previous studies establishing such an effect of *CDKN2A* knockdown in liver (11, 12). This suggests a possible contribution of the PKA-dependent potentiating pathway to the secretory

198 effects observed in the EndoC-bH1 cell line. Taken in combination with existing data, our
199 clinical and cellular studies indicate that the phenotype of carriers may arise out of a complex
200 interplay between both cell-cycle independent and dependent roles of *CDKN2A* in a range of
201 tissues (**supplementary figure 7)** (9, 12).

202 Upstream of the *CDKN2A* and *CDKN2B* genes, several independent association
203 signals for type 2 diabetes risk have been identified. The underlying effector transcript and
204 disease mechanism has remained elusive, and prior studies have not reported any cis-
205 expression quantitative trait loci (cis-eQTL) effects for these alleles (24). Our study has
206 shown that both coding *CDKN2A* mutations and the non-coding type 2 diabetes variants are
207 associated with effects on measures of β-cell function. This provides a link between
208 *CDKN2A* and the common GWAS alleles, and thus points to the gene as a likely effector
209 transcript at this locus.

210 Interestingly, type 2 diabetes-associated variants at the *CDKN2A/B* locus have
211 consistently been linked to a more 'classic' β-cell phenotype than that observed for carriers of
212 coding mutations in our study, with no evidence for an impact on measures of insulin
213 resistance (3, 4). We speculated that any cis-regulatory effect exerted on *CDKN2A* could
214 achieve a more restricted β-cell phenotype through tissue-specific regulation of gene
215 expression. To address this hypothesis, we interrogated existing genome annotations, and
216 found that the non-coding disease-associated variants map to a cluster of islet enhancer
217 activity and open chromatin. Specifically, the association signals overlap a strong enrichment
218 for islet- and melanocyte-specific FOXA-2 binding (**supplementary figure 8**) (25). This
219 highlights a possible mechanism for the more specific β-cell phenotype caused by common
220 disease-associated variants compared with carriers of coding variants. Based on the direction
221 of effect on measures of β-cell function, the non-coding risk alleles would be predicted to
222 increase expression of *CDKN2A* (3, 4). No cis-eQTL effects have previously been reported in

223 islets for this region, but larger studies currently underway may be able to shed further light
224 on this hypothesis (26).

225 Taken together, our data establish *CDKN2A* as an important regulator of glucose
226 homeostasis in humans. We have shown that our data are consistent with loss-of-function
227 mutations in *CDKN2A* affecting a range of tissues, including both pancreatic β-cells and
228 liver. Our study thus supports the candidacy of *CDKN2A* as the effector transcript of the type
229 2 diabetes-associated alleles in the region, and we have proposed a mechanism to account for
230 the apparent tissue-specificity of the β-cell dysfunction caused by diabetes risk alleles.

Acknowledgements

The authors thank Linda Whitaker (University of Leeds) and Beryl Barrow (University of Oxford) for their valuable assistance with recruiting FAMMM patients in the UK, Marja Dijk, Bep Ladan and Petra Beckers (Leiden University Medical Centre) for assistance with performing the OGTTs in the Netherlands, and Jonathan Levy (University of Oxford) for advice on designing the study. We thank all volunteers in the UK and the Netherlands for their participation. The Oxford Biobank (www.oxfordbiobank.org.uk), NIHR Oxford Biomedical Research Centre, is part of the NIHR National Bioresource which supported the recalling process of the volunteers.

This study was funded by the Wellcome Trust (095101/Z/10/Z and 098381), the Medical Research Council (G0800467), the National Institute of Health Research Oxford Biomedical Research Centre, Cancer Research UK (C588/A19167) and the ZOLEON foundation (no 12.09). ALG is a Wellcome Trust Senior Fellow in Basic Biomedical Science and MIM is a Wellcome Trust Senior Investigator. ALG is the guarantor of the data in this manuscript. The authors declare no conflicts of interest.

Author Contributions

AP, SKT, JNB, MIM, ALG conceived and designed the study. RS, TB provided protocols & clinical data. AP, TPP, SKT, AB, HJN performed the experiments. AP, ST, HJN, IFG analysed the data. AP, TPP, SKT, FK, IFG, HFAV, HP, MIM, ALG interpreted the data. SKT, ALG wrote the first draft of the manuscript. AP, TPP, MIM, HP edited the manuscript. AP, TPP, SKT, AB, HJN, RS, TJJ, IFG, TB, FK, HFAV, JNB, HP, MIM, ALG approved the final manuscript.

References

1 Voight, B.F., *et al.* (2010) Twelve type 2 diabetes susceptibility loci identified through large-scale association analysis. *Nat Genet* 42, 579-589
2 Morris, A.P., *et al.* (2012) Large-scale association analysis provides insights into the genetic architecture and pathophysiology of type 2 diabetes. *Nat Genet* 44, 981-990
3 Grarup, N., *et al.* (2007) Studies of association of variants near the HHEX, CDKN2A/B, and IGF2BP2 genes with type 2 diabetes and impaired insulin release in 10,705 Danish subjects: validation and extension of genome-wide association studies. *Diabetes* 56, 3105-3111
4 Dimas, A.S., *et al.* (2014) Impact of type 2 diabetes susceptibility variants on quantitative glycemic traits reveals mechanistic heterogeneity. *Diabetes* 63, 2158-2171
5 Kamb, A., *et al.* (1994) A cell cycle regulator potentially involved in genesis of many tumor types. *Science* 264, 436-440
6 Kamijo, T., *et al.* (1997) Tumor suppression at the mouse INK4a locus mediated by the alternative reading frame product p19ARF. *Cell* 91, 649-659
7 Serrano, M., *et al.* (1993) A new regulatory motif in cell-cycle control causing specific inhibition of cyclin D/CDK4. *Nature* 366, 704-707
8 Weber, H.O., *et al.* (2002) Human p14(ARF)-mediated cell cycle arrest strictly depends on intact p53 signaling pathways. *Oncogene* 21, 3207-3212
9 Krishnamurthy, J., *et al.* (2006) p16INK4a induces an age-dependent decline in islet regenerative potential. *Nature* 443, 453-457
10 Rane, S.G., *et al.* (1999) Loss of Cdk4 expression causes insulin-deficient diabetes and Cdk4 activation results in beta-islet cell hyperplasia. *Nat Genet* 22, 44-52
11 Lee, Y., *et al.* (2014) Cyclin D1-Cdk4 controls glucose metabolism independently of cell cycle progression. *Nature* 510, 547-551
12 Bantubungi, K., *et al.* (2014) Cdkn2a/p16Ink4a regulates fasting-induced hepatic gluconeogenesis through the PKA-CREB-PGC1alpha pathway. *Diabetes* 63, 3199-3209
13 Martin, J., *et al.* (2003) Genetic rescue of Cdk4 null mice restores pancreatic beta-cell proliferation but not homeostatic cell number. *Oncogene* 22, 5261-5269
14 Fiaschi-Taesch, N., *et al.* (2009) Survey of the human pancreatic beta-cell G1/S proteome reveals a potential therapeutic role for cdk-6 and cyclin D1 in enhancing human beta-cell replication and function in vivo. *Diabetes* 58, 882-893
15 Fiaschi-Taesch, N.M., *et al.* (2010) Induction of human beta-cell proliferation and engraftment using a single G1/S regulatory molecule, cdk6. *Diabetes* 59, 1926-1936
16 Cannon-Albright, L.A., *et al.* (1992) Assignment of a locus for familial melanoma, MLM, to chromosome 9p13-p22. *Science* 258, 1148-1152
17 Goldstein, A.M. (2004) Familial melanoma, pancreatic cancer and germline CDKN2A mutations. *Hum Mutat* 23, 630
18 Godsland, I.F., *et al.* (2006) Evaluation of nonlinear regression approaches to estimation of insulin sensitivity by the minimal model with reference to Bayesian hierarchical analysis. *Am J Physiol Endocrinol Metab* 291, E167-174
19 Ravassard, P., *et al.* (2011) A genetically engineered human pancreatic beta cell line exhibiting glucose-inducible insulin secretion. *J Clin Invest* 121, 3589-3597
20 Horwitz, D.L., *et al.* (1975) Proinsulin, insulin, and C-peptide concentrations in human portal and peripheral blood. *J Clin Invest* 55, 1278-1283
21 McKenzie, H.A., *et al.* (2010) Predicting functional significance of cancer-associated p16(INK4a) mutations in CDKN2A. *Hum Mutat* 31, 692-701
22 Keller-Melchior, R., *et al.* (1998) Expression of the Tumor Suppressor Gene Product p16INK4 in Benign and Malignant Melanocytic Lesions. 110, 932-938
23 Shanik, M.H., *et al.* (2008) Insulin resistance and hyperinsulinemia: is hyperinsulinemia the cart or the horse? *Diabetes Care* 31 Suppl 2, S262-268
24 Hannou, S.A., *et al.* (2015) Functional genomics of the CDKN2A/B locus in cardiovascular and metabolic disease: what have we learned from GWASs? *Trends Endocrinol Metab* 26, 176-184
25 Pasquali, L., *et al.* (2014) Pancreatic islet enhancer clusters enriched in type 2 diabetes risk-associated variants. *Nat Genet* 46, 136-143
26 Fadista, J., *et al.* (2014) Global genomic and transcriptomic analysis of human pancreatic islets reveals novel genes influencing glucose metabolism. *Proc Natl Acad Sci U S A* 111, 13924-13929

	Mutation carriers	Non-carriers	P-value
n	31	31	*NA*
BMI / [cm/kg^2]	27.1 [19; 38]	27.1 [19; 36]	0.97
Age / [yrs]	51.8 [21; 71]	51.8 [25; 84]	0.99
Gender / [% male]	45	32	0.43

Table 1 Baseline characteristics of study participants. Data are given as mean and range [min; max]. P-values are from Welch's t-test except for gender distribution where the Chi-squared test was performed.

	Mutation carriers	Non-carriers	P-value
Fasting glucose [mmol/L]	5.2 [4.3; 6.3]	5.1 [3.2; 6.4]	0.65
Fasting insulin [pmol/L]	87 [15; 337]	55 [22; 150]	0.01
Fasting C-peptide [nmol/L]	0.44 [0.24; 0.81]	0.39 [0.20; 0.60]	0.48
iHOMA-B	124 [38.1; 452.4]	96 [45; 236.7]	0.05
iHOMA-S	91 [18; 328.7]	120 [35; 235.6]	0.05
BIGTT-AIR [$*10^3$]	6.4 [0.9; 28]	3.0 [1.2; 12]	0.03
BIGTT-S	5.8 [0.4; 12.8]	7.8 [1.1; 17.8]	0.04
Belfiore ISI	0.78 [0.17; 1.35]	0.97 [0.35; 1.77]	0.02
Matsuda ISI	4.3 [0.8; 11.1]	6.3 [1.5; 20.9]	0.02
$AUC_{glucose}$	839 [563; 1449]	829 [502; 1086]	0.79
$AUC_{insulin}$ [$*10^4$]	7.3 [2.4; 25]	4.7 [1.1; 15]	0.01
$AUC_{C\text{-}Peptide}$	212 [106; 333]	212 [115; 260]	1.00
Insulinogenic index	203 [39; 561]	152 [53; 360]	0.08
C-peptidogenic index	0.45 [0.15; 1.12]	0.45 [0.17; 1.78]	1.00
Disposition index	2.3 [1.1; 3.8]	2.3 [1.0; 3.7]	0.98
Fasting insulin clearance	0.66 [0.12; 1.27]	0.88 [0.65; 1.29]	0.07
Insulin clearance	0.35 [0.16; 0.51]	0.56 [0.32; 1.05]	0.03

Table 2 OGTT-derived measures of β-cell function, insulin sensitivity and hepatic clearance. Data are given as mean and range [min; max]. All indices based on C-peptide measurements are based on data from a subset of individuals only (n = 12 carriers and n = 12 controls; all UK). Details on definitions of physiological measures are listed in supplementary table 2.

Figure legends

Figure 1 Serum glucose (*left panel*) and insulin (*right panel*) levels during a 120-min OGTT in thirty-one carriers (*black squares, solid line*) and thirty-one controls (*white circles, dashed line*). Data shown as mean +/- SEM.

Figure 2 *CDKN2A* knockdown in the human β-cell line, EndoC-bH1. Silencing of *CDKN2A* (*white bars*) and non-targeting sequence (*black bars*) was performed using pools of siRNA (10 nM), and knockdown confirmed both at the mRNA level (*upper left panel*) and at the protein level (*upper right panel*) after 72 h. Static insulin secretion assays were performed under culturing conditions of basal glucose (2.8 mM glucose), high glucose (20 mM) and high glucose with IBMX (100 μM) (*lower left panel*). All secretion results were normalized to total insulin content per well. Cellular proliferation (*lower right panel*) following treatment with si-*CDKN2A* (*white circles, dashed line*) and non-targeting siRNA (*black squares, solid line*) was measured using the CyQUANT Direct Cell Proliferation assay, and normalized to the respective counts on day 1. Bars represent means for n = 11 (si-*CDKN2A*) and 18 (non-targeting) generated in three independent experiments. Data points for cellular proliferation are means for n = 3, and error bars are SEM.

Figure 1

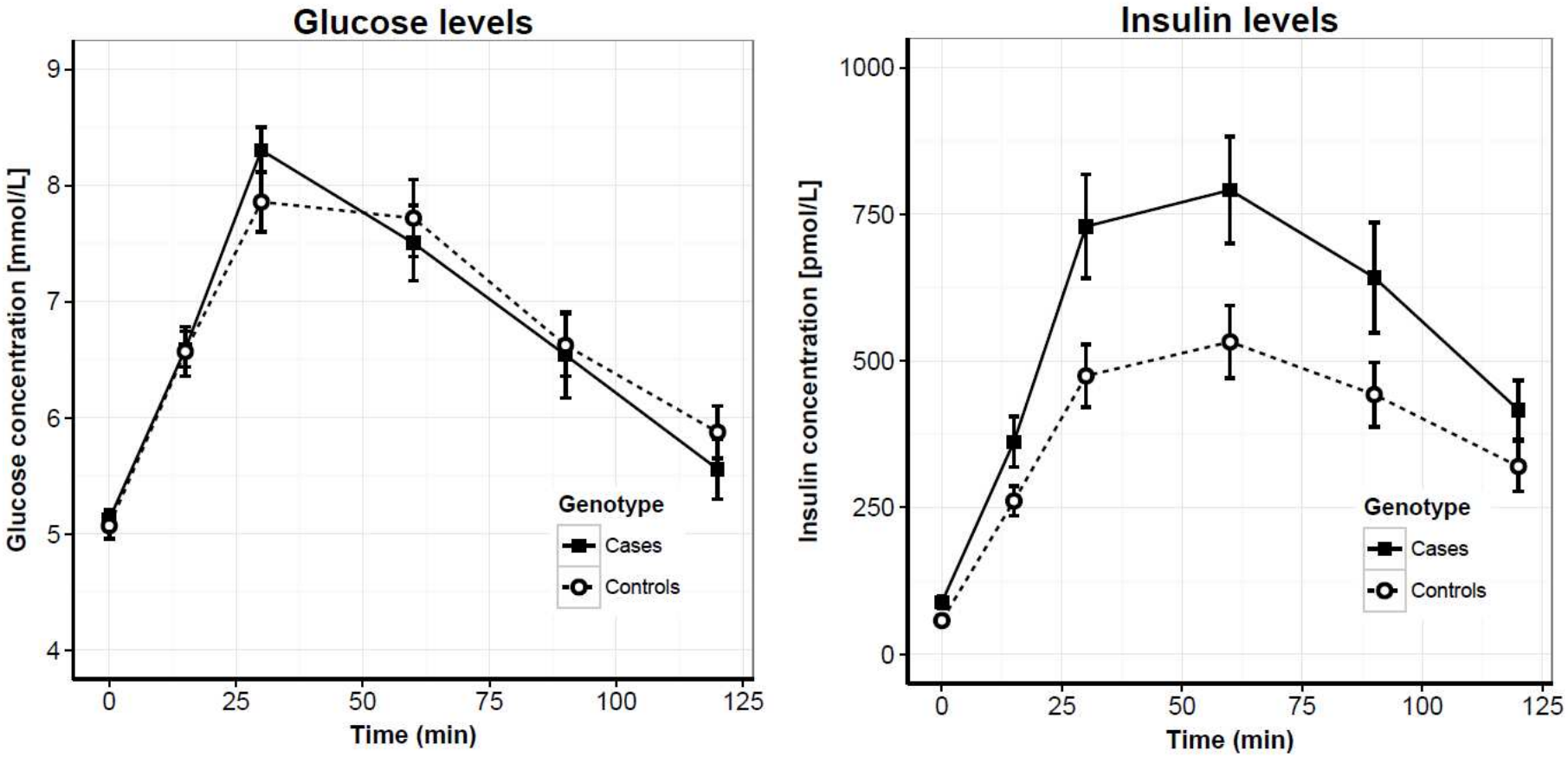
Glucose levels
Glucose concentration [mmol/L]
9
8
7
6
5
4
0
25
50
75
100
125
Time (min)
Genotype
Cases
Controls
Insulin levels
Insulin concentration [pmol/L]
1000
750
500
250
0
0
25
50
75
100
125
Time (min)
Genotype
Cases
Controls

Figure 2

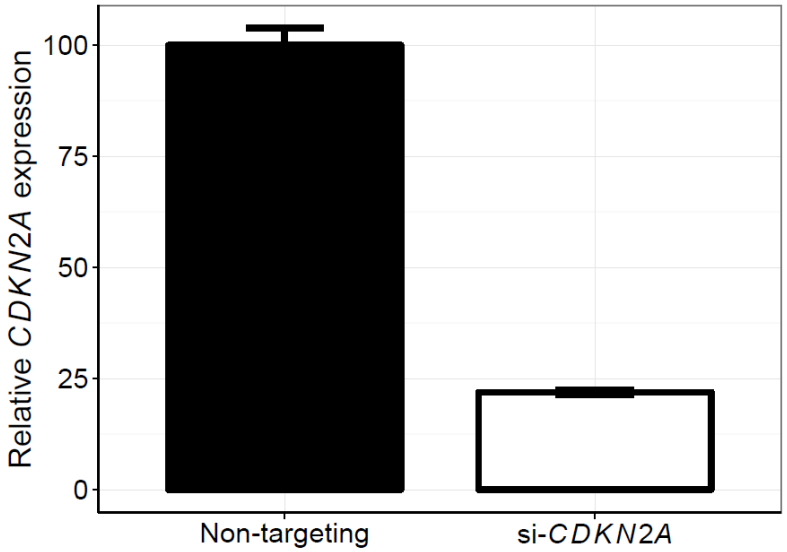
Relative CDKN2A expression
100
75
50
25
0
Non-targeting
si-CDKN2A

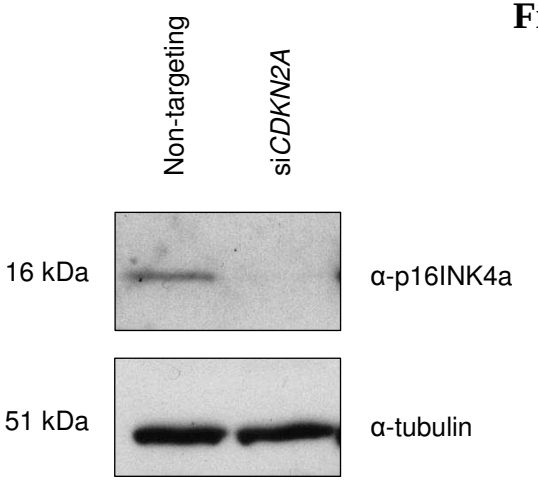
Non-targeting
siCDKN2A
16 kDa
α-p16INK4a
51 kDa
α-tubulin

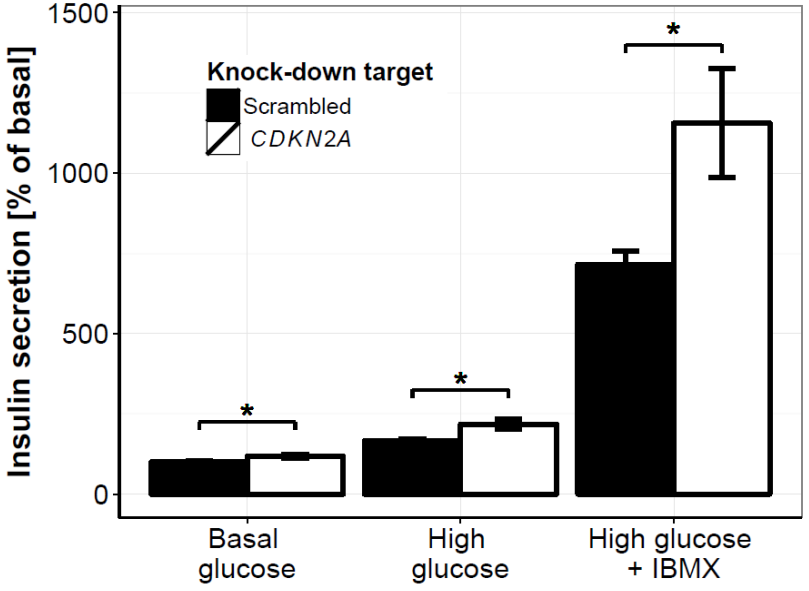
Insulin secretion [% of basal]
1500
1000
500
0
Knock-down target
Scrambled
CDKN2A
*
*
*
Basal glucose
High glucose
High glucose + IBMX

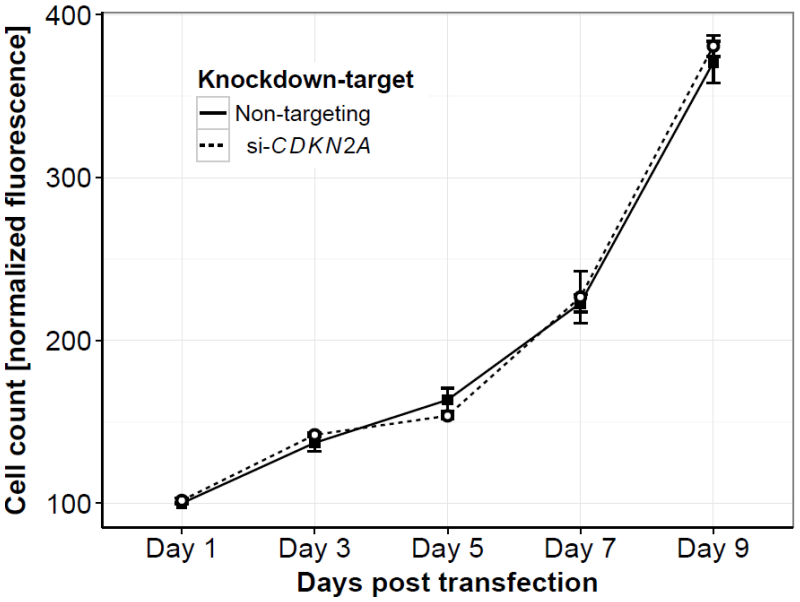
Cell count [normalized fluorescence]
400
300
200
100
Knockdown-target
Non-targeting
si-CDKN2A
Day 1
Day 3
Day 5
Day 7
Day 9
Days post transfection

Supplementary online information

Participant ID	Transcript affected	Mutation	Melanoma-free for > 2 years prior to study	Variant Effect Predictor (VEP - Ensembl)
OX_001	P16-INK4a only	c.88delG	Yes	Frameshift variant
OX_002	P16-INK4a only	c.88delG	Yes	Frameshift variant
OX_003	P16-INK4a only	c.88delG	Yes	Frameshift variant
OX_004	Both	c.458-105A>G	Yes	Intronic variant
OX_005	Both	c.458-105A>G	Yes	Intronic variant
OX_006	Both	c.458-105A>G	Yes	Intronic variant
OX_007	P16-INK4a only	c.52_57dup	Yes	Protein altering variant
OX_008	P16-INK4a only	c.52_57dup	Yes	Protein altering variant
OX_009	Both	c.159G>A	Yes	Missense variant
OX_010	Both	c.159G>A	Yes	Missense variant
OX_011	Both	c.458-105A>G	Yes	Intronic variant
OX_012	Both	*Not tested*	Yes	*NA*
LEI_001	Both	c.225_243del19	No	Frameshift variant
LEI_002	Both	c.225_243del19	Yes	Frameshift variant
LEI_003	Both	c.225_243del19	Yes	Frameshift variant
LEI_004	Both	c.225_243del19	Yes	Frameshift variant
LEI_005	Both	c.225_243del19	Yes	Frameshift variant
LEI_006	Both	c.225_243del19	Yes	Frameshift variant
LEI_007	Both	c.225_243del19	Yes	Frameshift variant
LEI_008	Both	c.225_243del19	Yes	Frameshift variant
LEI_009	Both	c.225_243del19	Yes	Frameshift variant

LEI_010	Both	c.225_243del19	Yes	Frameshift variant
LEI_011	Both	c.67G>C	No	Missense variant
LEI_012	Both	c.225_243del19	No	Frameshift variant
LEI_013	Both	c.225_243del19	Yes	Frameshift variant
LEI_014	Both	c.225_243del19	Yes	Frameshift variant
LEI_015	Both	c.225_243del19	Yes	Frameshift variant
LEI_016	Both	c.225_243del19	Yes	Frameshift variant
LEI_017	Both	c.225_243del19	Yes	Frameshift variant
LEI_018	Both	c.225_243del19	Yes	Frameshift variant
LEI_019	Both	c.225_243del19	Yes	Frameshift variant

Supplementary table 1 List of mutations identified in carriers (annotated against CDKN2A-001 [ENST00000304494]) by targeted sequencing. The second column indicates whether the mutation maps to a region encoding just $p16^{INK4a}$ or both $p16^{INK4a}$ and $p14^{ARF}$. Participant ID is an anonymous number assigned to each case, and the prefix indicates from which cohort the patient was recruited (OX = Oxford, UK; LEI = Leiden, Netherlands).

Measure/index	Parameter	Formula or mathematical model used	Reference
iHOMA-B	Beta-cell function	Computer model available via (http://www.dtu.ox.ac.uk/homacalculator/).	(1)
iHOMA-S	Insulin sensitivity	Computer model available via (http://www.dtu.ox.ac.uk/homacalculator/).	(1)
BIGTT-AIR$_{0\text{-}30\text{-}120}$	Beta-cell function	exp[8.20 + (0.00178 * insulin$_0$) + (0.00168 * insulin$_{30}$) -(0.000383 * insulin$_{120}$) - (0.314 * glucose$_0$) - (0.109 * glucose$_{30}$) + (0.0781 * glucose$_{120}$) + (0.180 * gender (where male=0 and female=1)) - (0.032 * BMI)]	(2)
BIGTT-$S_{I\_0\text{-}30\text{-}120}$	Insulin sensitivity	exp[4.90 - (0.00402 * insulin$_0$) - (0.000556 * insulin$_{30}$) -(0.00127 * insulin$_{120}$) - (0.152 * glucose$_0$) - (0.00871 * glucose$_{30}$) - (0.0373 * glucose$_{120}$) - (0.145 * gender (where male=0 and female=1)) - (0.0376 * BMI)]	(2)
Belfiore ISI	Insulin sensitivity	2/[(0.5 * glucose$_0$ + glucose$_{60}$ + 0.5 * glucose$_{120}$)/11.36) * (0.5* insulin$_0$ + insulin$_{60}$ + 0.5* insulin$_{120}$)/638) + 1]	(3)
Matsuda ISI	Insulin Sensitivity	10 000 * √(glucose$_0$* insulin$_0$ * glucose$_{mean\text{-}OGTT}$ * insulin$_{mean\text{-}OGTT}$)	(4)
AUC	Multiple	Area under curve estimated using trapezoidal rule	(5)
Insulinogenic index	Beta-cell function	(insulin$_{30}$ – insulin$_0$)/(glucose$_{30}$ - glucose$_0$)	(6)
Disposition index	Beta-cell function	AUC$_{insulin\text{-}OGTT}$/AUC$_{glucose\text{-}OGTT}$ * Matsuda ISI	(6)
Hepatic insulin clearance	Insulin clearance	AUC$_{C\text{-}Peptide}$/AUC$_{Insulin}$	(7)
Fasting insulin clearance	Insulin clearance	C-peptide$_0$/insulin$_0$	(7)

Supplementary table 2 Definitions of physiological measurements and indices derived from the OGTT. Subscripts denote time points during the OGTT. Units are pmol/L for insulin, nmol/L for C-peptide and mmol/L for glucose, except in the case of Matsuda ISI and the disposition index, where glucose was inputted in units of mg/dL and insulin as μU/mL.

	Mutation carriers	Non-carriers	P-value
n	28	31	*NA*
BMI [cm/kg^2]	27 [19, 38]	27 [19, 37]	0.66
Age [yrs]	51 [21, 71]	52 [25, 84]	0.96
Gender [% male]	43	33	0.58
Fasting glucose [mmol/L]	5.1 [4.3, 6.3]	5.1 [3.2, 6.4]	0.92
Fasting insulin [pmol/L]	91 [15, 337]	57 [22, 150]	0.01
iHOMA-B	133 [38, 452]	99 [45, 237]	0.03
iHOMA-S	86 [18, 329]	116 [35, 236]	0.04
BIGTT-AIR [*10^3]	6.6 [0.9, 28]	3.2 [1.2, 12]	0.03
BIGTT-S	5.8 [0.4, 12.7]	7.5 [1.1, 17.8]	0.08
Belfiore ISI	0.80 [0.17, 1.35]	0.96 [0.35, 1.77]	0.03
Matsuda ISI	4.3 [0.8; 11.1]	6.1 [1.5; 20.9]	0.02
$AUC_{glucose}$	831 [563, 1449]	832 [502, 1086]	0.98
$AUC_{Insulin}$ [*10^4]	7.2 [2.4, 25]	4.9 [1.1, 15]	0.02
Insulinogenic index	205 [39, 561]	155 [53, 360]	0.10
Disposition index	2.3 [1.1, 3.8]	2.3 [1.0, 3.7]	0.92

Supplementary table 3 Comparison of OGTT-derived measures for carriers and non-carriers after exclusion of three subjects that had presented with cancer within two years prior to the study (supplementary table 1). Data are given as mean and range [min; max], and p-values are from Welch's t-test, except for gender distribution where the Chi-squared test was performed. Details on definitions of physiological measures are listed in supplementary table 2. * P-value < 0.05.

	Mutation carriers	Non-carriers	P value
n	8	8	*NA*
$AUC_{insulin}$ 0-10 min (pmol.L^{-1}.min*10^{-3})	4.8 [1.73, 13.2]	2.9 [1.84, 4.28]	0.51
$AUC_{insulin}$ 10-180 min (pmol.L^{-1}.min*10^{-3})	35.5 [13.7, 94.9]	16.9 [12.5, 22.2]	0.16
$AUC_{C\text{-}peptide}$ 0-10 min (pmol.L^{-1}.min*10^{-3})	15.1 [9.1, 31.9]	11.7 [5.5, 14.5]	0.96
$AUC_{C\text{-}peptide}$ 10-180 min (pmol.L^{-1}.min*10^{-3})	198 [103, 364]	152 [101, 186]	1.00
Net IVGTT insulin secretion 0-10 min (pmol.L^{-1})	0.56 [0.29, 0.84]	0.50 [0.10, 1.04]	0.65
Net IVGTT insulin secretion 10-180 min (pmol.L^{-1})	4.2 [1.20, 11.8]	2.8 [1.10, 4.98]	0.65
Insulin sensitivity, S_I (min^{-1}.$pmol^{-1}$.L)	0.72 [0.19, 1.28]	0.68 [0.30, 0.95]	0.72
Disposition index [*10^{-3}]	2.4 [1.14, 4.44]	1.9 [0.77, 3.40]	0.51
C-peptide disposition index	8.9 [3.45, 12.6]	7.8 [4.00, 13.7]	0.80
Fractional hepatic insulin throughput	0.53 [0.34, 1.12]	0.41 [0.26, 0.74]	0.23
Plasma insulin elimination rate (min^{-1})	0.098 [0.025, 0.207]	0.095 [0.042, 0.235]	0.72

Supplementary table 4 IVGTT-derived measures of β-cell function, insulin sensitivity and hepatic clearance. Data are given as mean and range [min; max]. All p-values are based on Mann-Whitney U test.

Supplementary figure legends

Supplementary figure 1 Serum glucose (*left panel*) and insulin (*right panel*) levels during a 120-min OGTT in twenty-six cases with *CDKN2A* loss-of-function mutations affecting both $p16^{INK4a}$ and $p14^{ARF}$ (*black triangles, dotted line*), five cases with *CDKN2A* loss-of-function mutations affecting $p16^{INK4a}$ exclusively (*black squares, solid line*), and thirty-one BMI-, age-, and gender-matched controls (*white circles, dashed line*). Data shown as mean +/- SEM.

Supplementary figure 2 Serum glucose (*left panel*) and insulin (*right panel*) levels during a 180-min IVGTT in eight carriers (*pink circles*) and eight BMI- ($p = 0.72$), age- ($p = 0.96$), and gender-matched ($p = 0.50$) controls (*blue squares*). Data shown as mean +/- SEM.

Supplementary figure 3 Immunofluorescence staining of p16INK4a (Abcam, ab81278; recognizing isoform 1 of the protein) in the human beta-cell line, EndoC-bH1. In siRNA-mediated knockdown experiments, expression of p16INK4a protein was visibly down-regulated (*bottom panel*) as compared with control cells (*top panel*). Cell nuclei were stained using NucRed Dead 647 (Life Technologies). Images were taken on a BioRad Radiance 2100 confocal microscope with a 60X 1.0 N.A. objective, and the same laser settings and intensities were used across samples. Scale bar, 20 μm.

Supplementary figure 4 Gene expression profiles of critical cell-cycle regulators after silencing of *CDKN2A* in the human β-cell line, EndoC-bH1. Knockdown experiments were performed as described for figure 2. Relative gene expression of *CDK4* (*top left*), *CDK6* (*top right*), *CDKN2A* (*bottom left*) and *CDKN2B* (*bottom right*) corrected for expression of two housekeepers using the delta-delta Ct method, and normalized to non-targeting control. As shown, we observed efficient knockdown of CDKN2A with no off-target effect on the *CDKN2B* gene. Bars represent means for n = 4-5 and error bars are SEM.

Supplementary figure 5 Insulin content normalized to cell-count following *CDKN2A* knockdown. After static insulin secretion assays, cells were counted and insulin contents extracted as described in figure 2. Using these data, the insulin content relative to the number of cells per well was calculated as the ratio between these two numbers, and normalized to scrambled control. Bars represent means for the aggregate of basal and high glucose measurements for n = 16, and error bars are SEM.

Supplementary figure 6 PKA activity in the EndoC-bH1 cell line following *CDKN2A* knockdown. 96 h after treatment with non-targeting ("scrambled"; *blue bar*) or *CDKN2A* (*red bar*) siRNAs, cells were harvested and PKA activity measured on sample input normalized to cell numbers. Substrate conversion rates were calculated as the ratio of non-phosphorylated to total peptide using fluorescence intensities quantified with standard software on the ChemiDoc MP system. Data shown as mean +/- SEM for three independent replicates.

Supplementary figure 7 Outline of two non-mutually exclusive mechanisms compatible with the phenotype of *CDKN2A* mutations-carriers. According to model 1 (*left*), a primary reduction in insulin sensitivity leads to a compensatory increase in insulin secretion to maintain glucose homeostasis. The effect of *CDKN2A*-loss would therefore be in non-beta cell tissues, such as liver. Model 2 (*right*), in contrast, represent the alternative scenario: chronically elevated insulin levels due to β-cell hypersecretion drives a progressive decrease in insulin receptors and insulin signalling through homologous desensitization (8). In this case, the primary effect of *CDKN2A* loss is on the pancreatic beta-cell, but the mechanism ultimately manifests as impaired insulin sensitivity and reduced insulin clearance. As discussed in the main text, it is likely that a combination of the two models contributes to both beta-cell hypersecretion and primary insulin resistance.

Supplementary figure 8 Screenshot from the Human Islet Regulome Browser (9) showing annotations of chromatin state, transcription factor binding and variant association with type 2 diabetes at the *CDKN2A/B locus*. The genomic binding sites of islet transcription factors (PDX1, NKX2.2, FOXA2, NKX6.1, MAFB) are indicated by lines connected to the respective proteins. A Manhattan plot above shows log(p-values) of association with type 2 diabetes for variants in the MAGIC (*blue*) and DIAGRAM (*red*) datasets (10, 11). Lead variants tagging the two genome-wide association signals located downstream of *CDKN2B-AS1* are shown. Fine-mapping efforts have since publication of the islet regulome narrowed down the number of potential causative variants to credible sets of five and six variants (Gaulton et al, (2015) Nature Genetics, *in press*). Both of these sets contain variants that directly overlap a FOXA2 binding site.

Supplementary references

1 Matthews, D.R., *et al.* (1985) Homeostasis model assessment: insulin resistance and beta-cell function from fasting plasma glucose and insulin concentrations in man. *Diabetologia* 28, 412-419
2 Hansen, T., *et al.* (2007) The BIGTT test: a novel test for simultaneous measurement of pancreatic beta-cell function, insulin sensitivity, and glucose tolerance. *Diabetes Care* 30, 257-262
3 Belfiore, F., *et al.* (1998) Insulin sensitivity indices calculated from basal and OGTT-induced insulin, glucose, and FFA levels. *Mol Genet Metab* 63, 134-141
4 Matsuda, M. and DeFronzo, R.A. (1999) Insulin sensitivity indices obtained from oral glucose tolerance testing: comparison with the euglycemic insulin clamp. *Diabetes Care* 22, 1462-1470
5 Pacini, G. and Mari, A. (2003) Methods for clinical assessment of insulin sensitivity and beta-cell function. *Best Pract Res Clin Endocrinol Metab* 17, 305-322
6 Phillips, D.I., *et al.* (1994) Understanding oral glucose tolerance: comparison of glucose or insulin measurements during the oral glucose tolerance test with specific measurements of insulin resistance and insulin secretion. *Diabet Med* 11, 286-292
7 Herzberg-Schafer, S.A., *et al.* (2010) Evaluation of fasting state-/oral glucose tolerance test-derived measures of insulin release for the detection of genetically impaired beta-cell function. *PLoS One* 5, e14194
8 Shanik, M.H., *et al.* (2008) Insulin resistance and hyperinsulinemia: is hyperinsulinemia the cart or the horse? *Diabetes Care* 31 Suppl 2, S262-268
9 Pasquali, L., *et al.* (2014) Pancreatic islet enhancer clusters enriched in type 2 diabetes risk-associated variants. *Nat Genet* 46, 136-143
10 Morris, A.P., *et al.* (2012) Large-scale association analysis provides insights into the genetic architecture and pathophysiology of type 2 diabetes. *Nat Genet* 44, 981-990
11 Voight, B.F., *et al.* (2010) Twelve type 2 diabetes susceptibility loci identified through large-scale association analysis. *Nat Genet* 42, 579-589

Supplementary figure 1

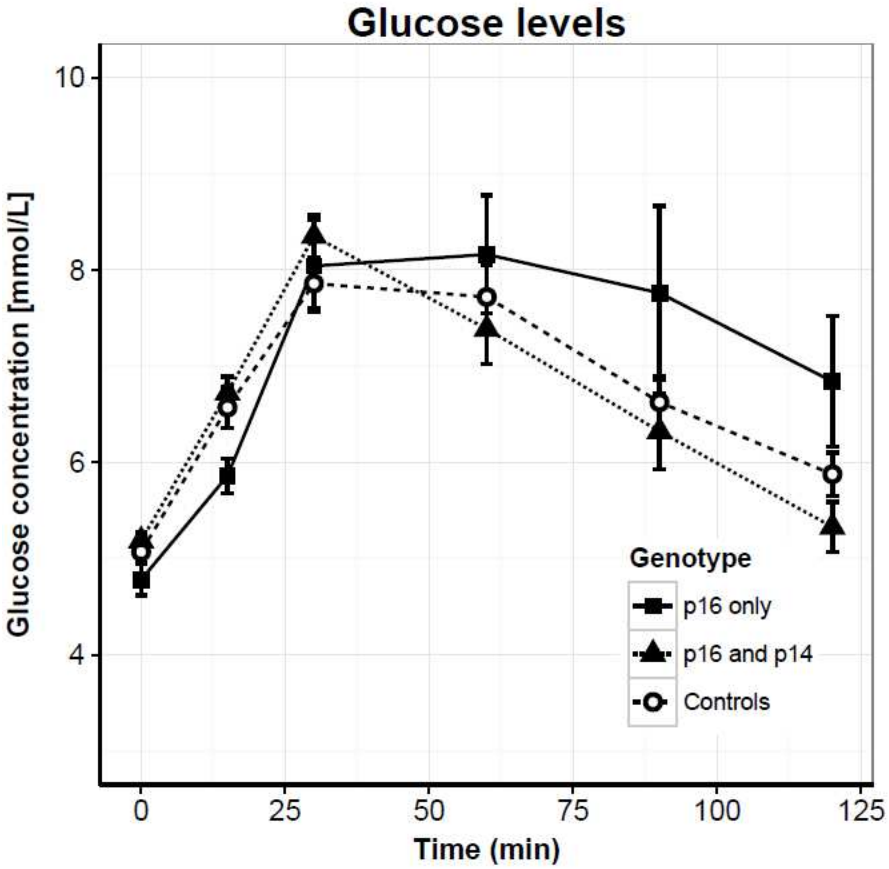

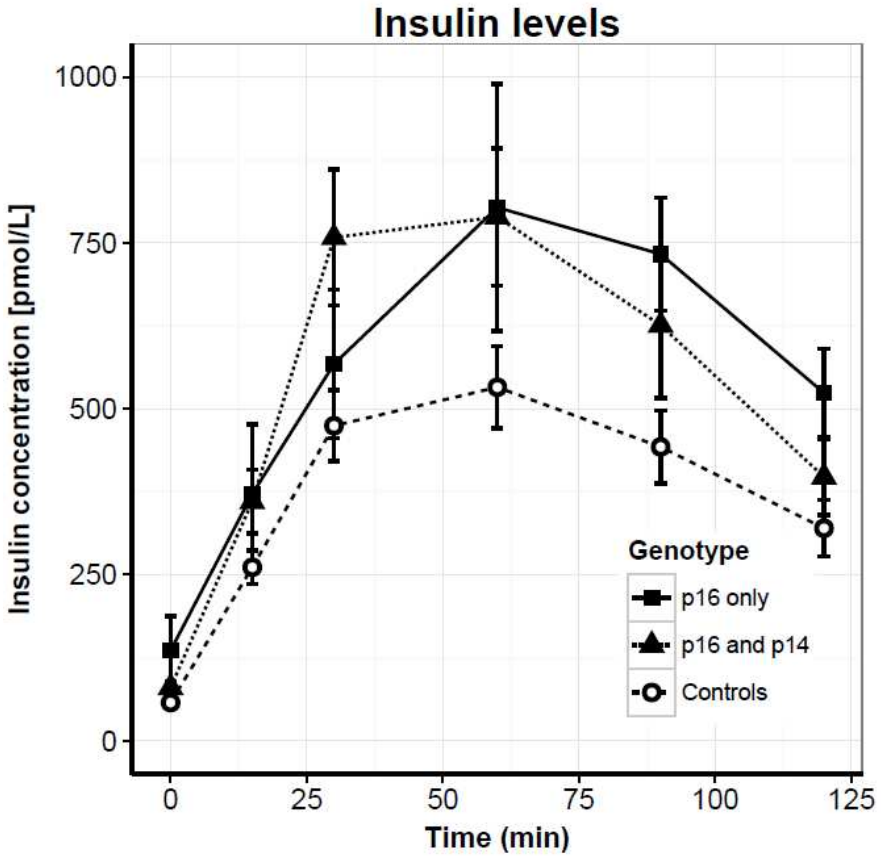

Supplementary figure 2

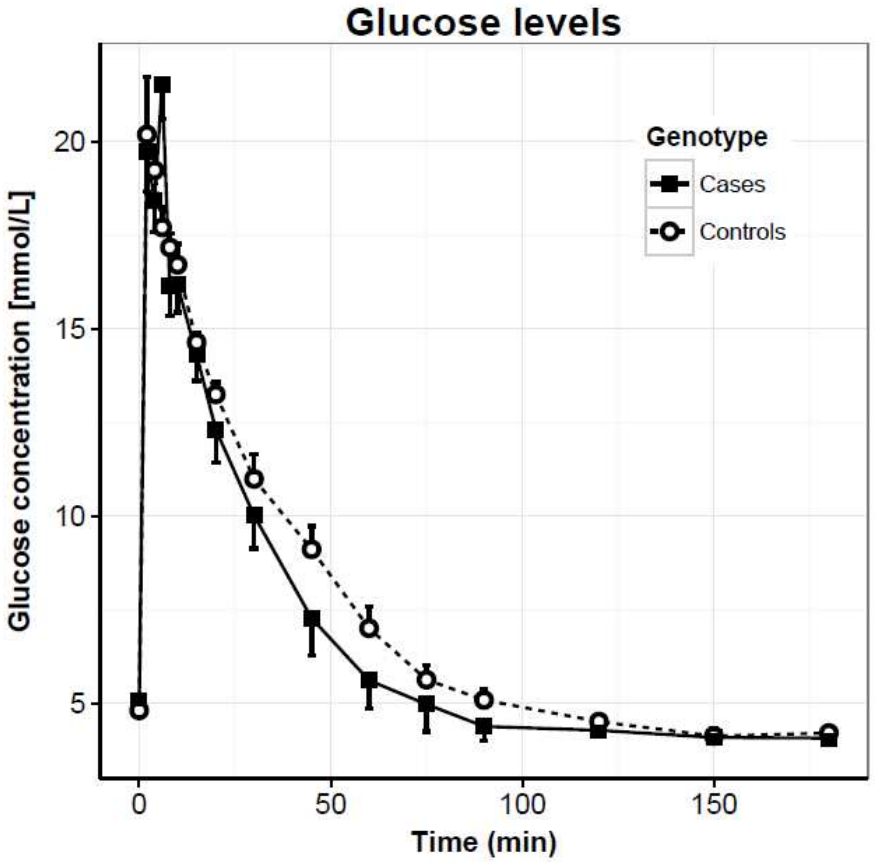

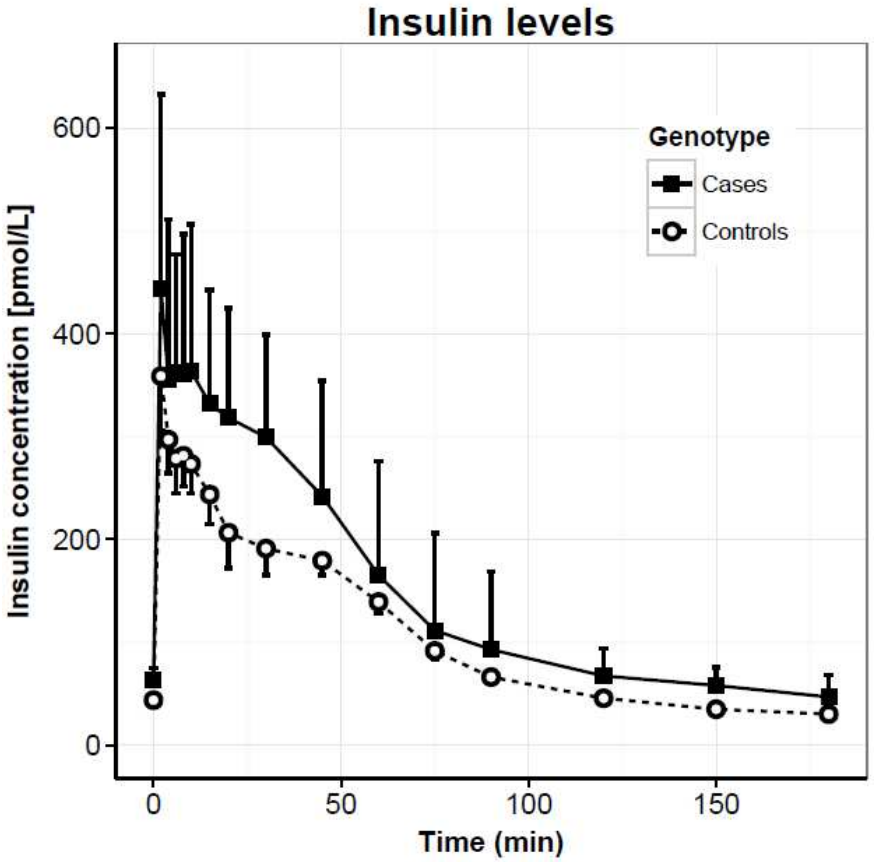

Supplementary figure 3

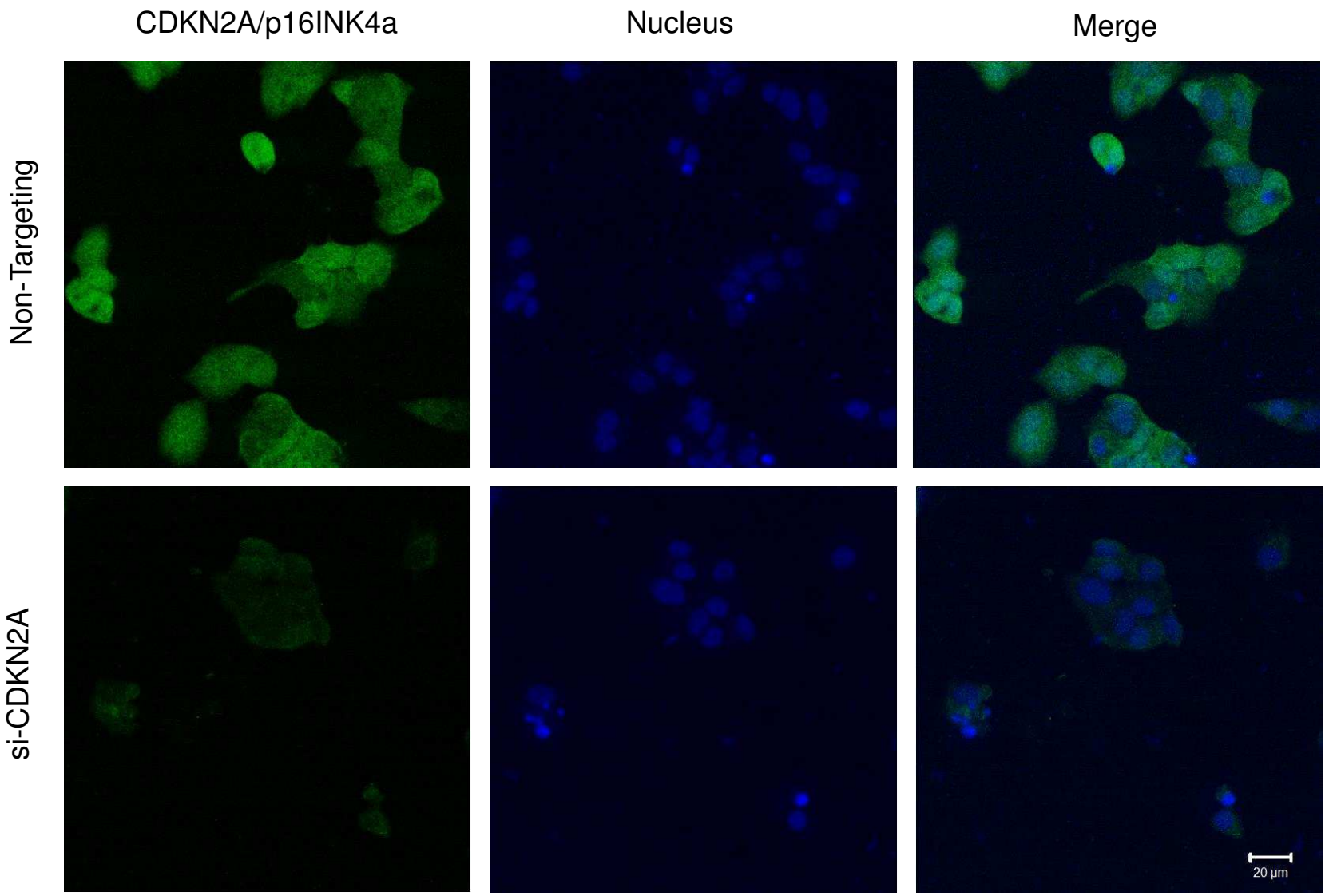

Supplementary figure 4

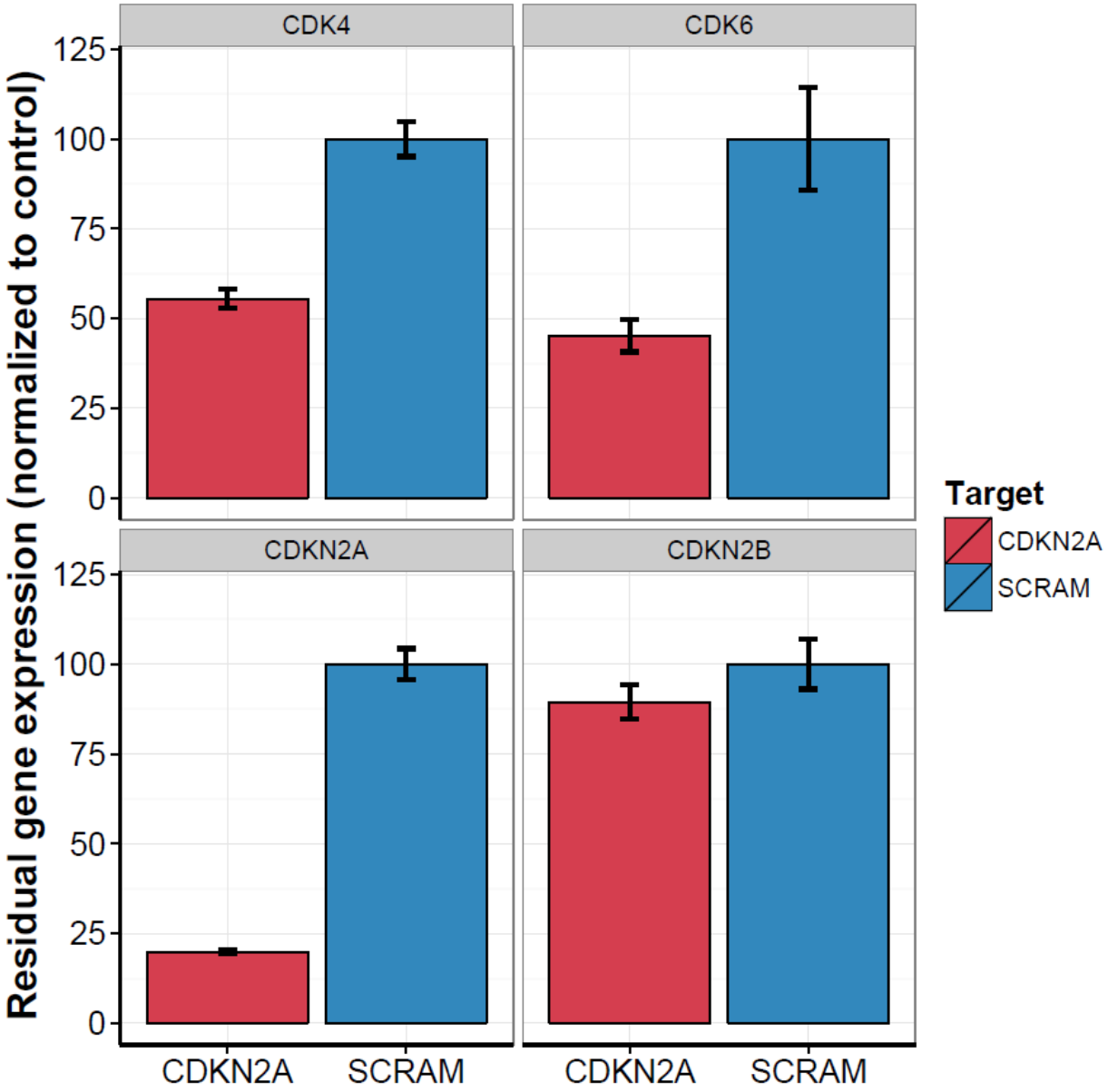

Supplementary figure 5

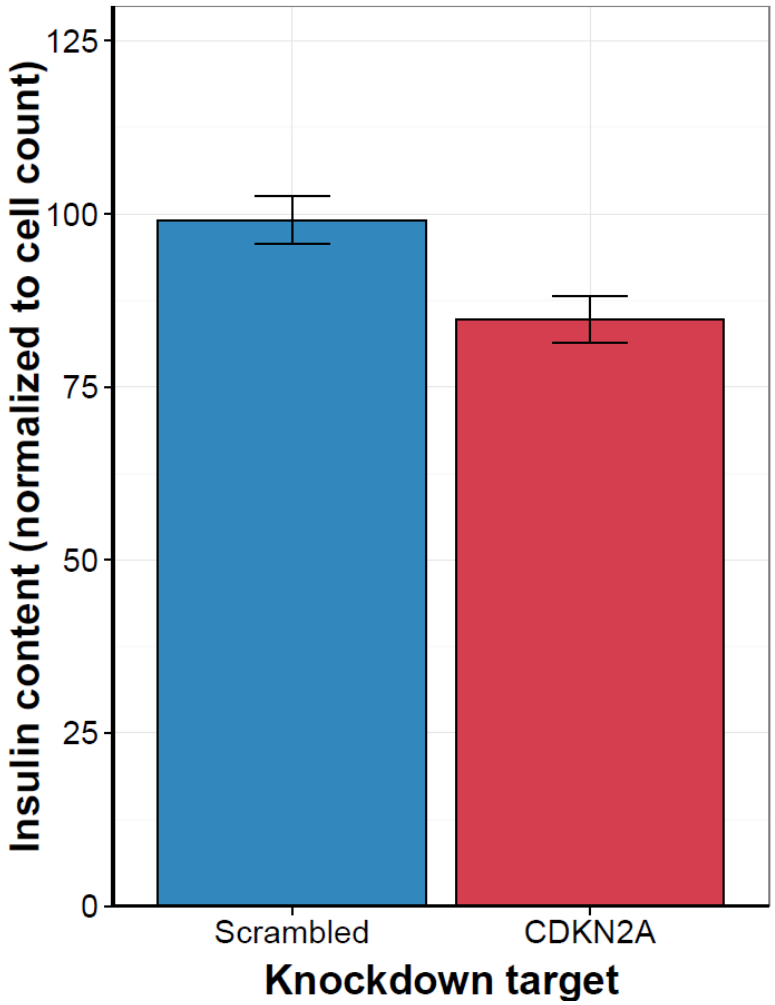

Supplementary figure 6

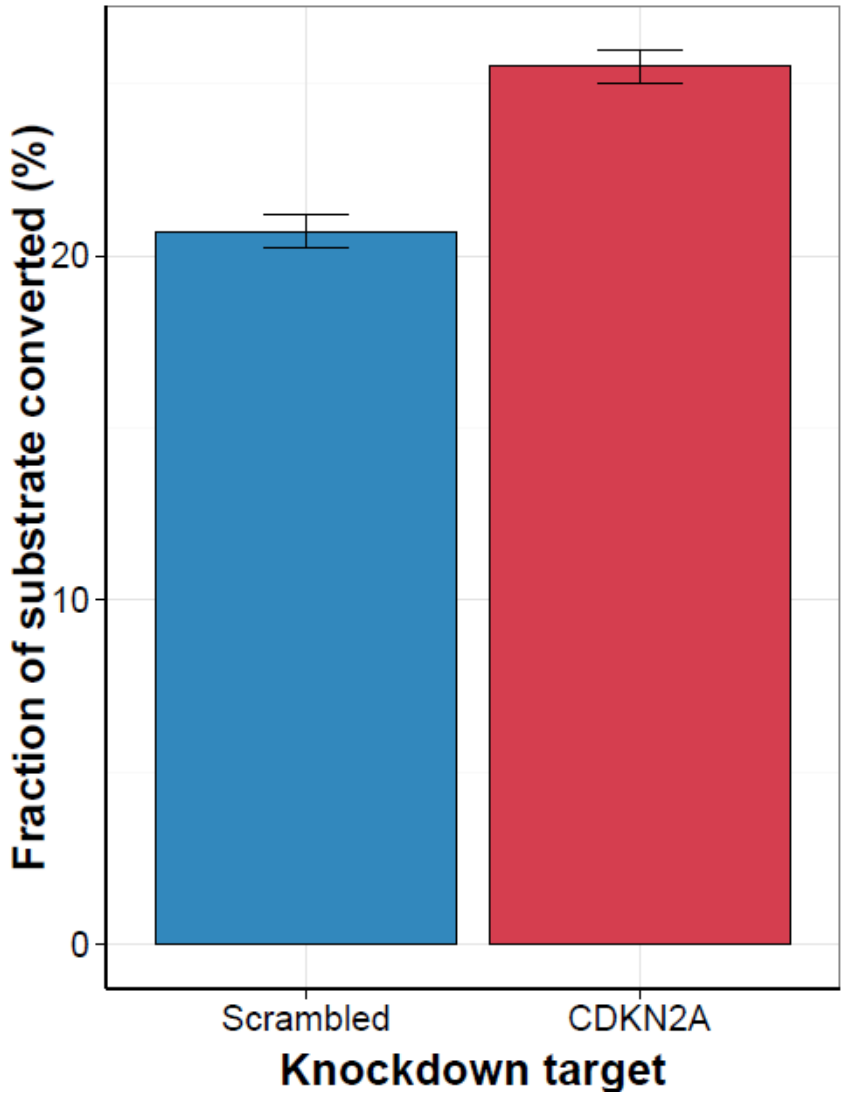

Supplementary figure 7

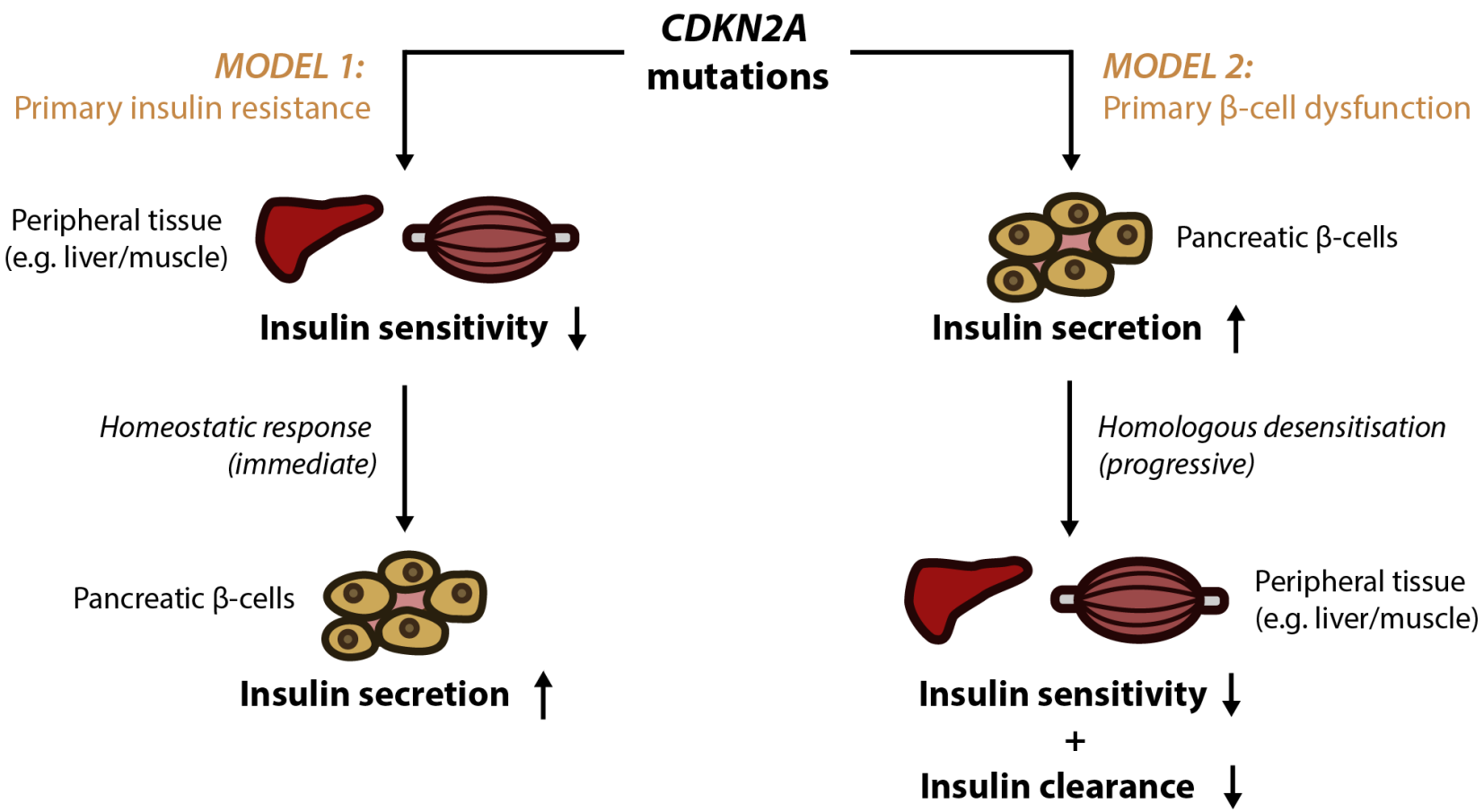

Supplementary figure 8